

# Journal of Materials Chemistry C

Accepted Manuscript



This is an *Accepted Manuscript*, which has been through the Royal Society of Chemistry peer review process and has been accepted for publication.

*Accepted Manuscripts* are published online shortly after acceptance, before technical editing, formatting and proof reading. Using this free service, authors can make their results available to the community, in citable form, before we publish the edited article. We will replace this *Accepted Manuscript* with the edited and formatted *Advance Article* as soon as it is available.

You can find more information about *Accepted Manuscripts* in the [Information for Authors](#).

Please note that technical editing may introduce minor changes to the text and/or graphics, which may alter content. The journal's standard [Terms & Conditions](#) and the [Ethical guidelines](#) still apply. In no event shall the Royal Society of Chemistry be held responsible for any errors or omissions in this *Accepted Manuscript* or any consequences arising from the use of any information it contains.

## Temperature-controlled Morphology Evolution of Porphyrin Nanostructures from Oil-aqueous Interface

Cite this: DOI: 10.1039/x0xx00000x

J. H. Cai<sup>a,c</sup>, T. Wang<sup>a</sup>, J. X. Wang,<sup>a\*</sup> Y. L. Song,<sup>b</sup> and L. Jiang<sup>a,b</sup>Received 00th January 2012,  
Accepted 00th January 2012

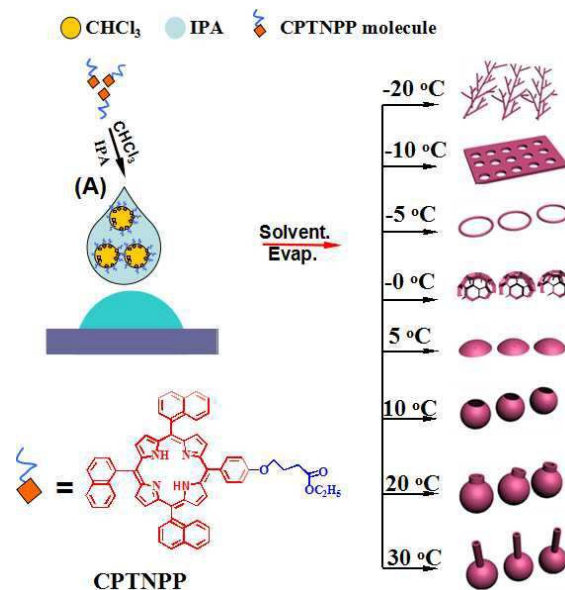
DOI: 10.1039/x0xx00000x

www.rsc.org/

Various porphyrin nanostructures including of tree-, wavy-, honey-comb, ring-, skeleton-, jar-, hollow spherical- and flask-like were facily fabricated on the hydrophilic substrate from oil-aqueous interface when varying the assembly temperature. It is of great significance for the design and creation of the porphyrin structure and its extended applications in optic devices.

Porphyrin nanostructures materials<sup>1-6</sup> with tunable morphology have become promising candidates for optic-electronics, including organic field-effect transistors,<sup>5d</sup> phototherapy and photodiagnostic<sup>1d</sup>, nanosensors<sup>5a</sup> and optic-limiting properties<sup>4d</sup> because of their unique architectures, tailored physicochemical properties based on the conjugated structure of porphyrin core.<sup>1,4-6</sup> To date, a paramount of organic nanostructures, such as nanofibers,<sup>1c</sup> nanorods,<sup>4b</sup> nanotubes,<sup>4c</sup> nanoprism<sup>3a</sup>, etc. have been formulated through various self-assembly protocols, including organogelation, interfacial assembly, molecular recognition, reprecipitation, surfactant-assisted self-assembly etc. These assembly approaches pay main emphasis on the modulation of molecular structure<sup>3c-d,4c</sup> or micro-environment<sup>4b</sup> (pH or sonication system<sup>4b</sup>). Few papers refer to controlling the assembly nanostructures from the modulated substrate wettability.<sup>6</sup> As matter of fact, substrate wettability has been proved to be an effective approach for the modulation of the aggregate morphology and molecule assembly.<sup>9-12</sup> Typically, ring-, wheel-, hole-shell porphyrin structures<sup>6a</sup> were facily fabricated by combining droplet template<sup>6-8</sup> and the effective modulation of the substrate's hysteresis properties. And a beautiful flower-shaped porphyrin Janus aggregate is swiftly obtained from the two-step droplet condensation process on the hydrophobic substrate.<sup>6b</sup> In this paper, we demonstrated a comprehensive morphology evolution from the porphyrin derivative by droplet template on hydrophilic substrate by just changing the assembly temperature. Porphyrin nanostructures covering tree-, wavy-, honey-comb, ring-, skeleton-, jar-, hollow spheric- and flask-like were facily obtained. The formation of nanostructures was attributed to the distinct dewetting behavior i.e., stick-slip mode of the three phase contact line (TCL) of the droplet template aroused from varying

the assembly temperature. The work would pose an important insight for the design and fabrication of the porphyrin nanostructures and the corresponding optic devices.



**Scheme 1.** Typical formation process of various porphyrin nanostructures from varying assembly temperature. The process includes the preparation of CPTNPP suspension, spreading the suspension onto the droplet on the hydrophilic substrate at different temperatures and the formation of the structure covering of tree-like, honey-comb, ring-, jar- and flask-like after solvent evaporation.

**Scheme 1** presents the typical formation process of porphyrin nanostructures assembled from the porphyrin derivative of 5-(4-(ethylcarboxypropoxy)phenyl)-10,15,20-tri(naphthyl) (CPTNPP, synthetic detail is in the supporting information). Firstly, the CPTNPP suspension is prepared by dissolving CPTNPP into the chloroform with a concentration of  $10^{-5}$ ~ $10^{-6}$  mol/L and subsequently adding the formed solution into isopropyl alcohol (IPA) in volume ratio of 1:1. In the process, the poor dissolution of CPTNPP in IPA makes the formation of

CPTNPP vesicles in the suspension (Figure S1), with hydrophobic porphyrin core toward the chloroform phase, and the hydrophilic ether group toward the IPA phase. Secondly, the porphyrin suspension was casted onto the droplet template produced on the hydrophilic substrate at -20, -10, -5, 0, 5, 10, 15, 20, and 30°C respectively as shown in Scheme S2. After solvent evaporation, various CPTNPP nanostructures were obtained based on the distinct assembly temperatures. The assembled morphology includes tree-like, honey-comb, ring-, jar- and flask-shaped structure.

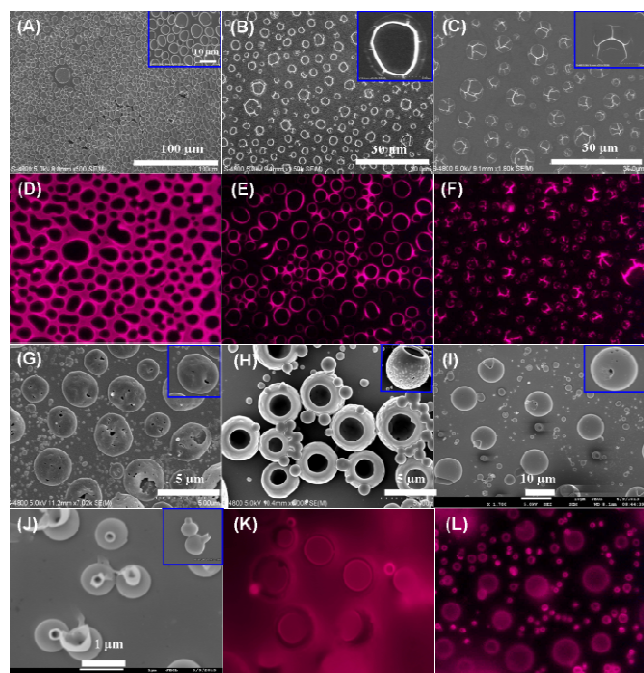


**Figure 1.** Typical SEM and fluorescent images of various porphyrin nanostructures assembled from different temperatures. (A, D) Honey-comb (-10°C), (B, E) Ring-shaped (-5°C), (C, F) Skeleton-like (0°C), (G) Hemi-spheric (5°C), (H, K) Jar-like (10°C), (I and L) Hollow-spherical (20°C) and (J) Flask-shaped (30°C) nanostructures.

**Figure 1** displays typical scanning electron microscope (SEM) and fluorescent images of porphyrin nanostructures assembled from different temperatures. Interestingly, various nanostructures were obtained when varying the assembly temperature. The tree-like structure is obtained at -20°C spanned hundreds of micrometer in Figure S3, its dimension is *ca.* 80  $\mu\text{m}$ . The wavy-like (Figure S4) or honey-comb (Figure 1A, 1D, Figure S5) structure is obtained at -10°C, its dimension is *ca.* 10  $\mu\text{m}$ . The ring- (Figure 1B, 1E, Figure S6), skeleton- (Figure 1C, 1F, Figure S7), and cap-like (Figure 1G), nanostructures are obtained at -5°C, 0°C and 5°C respectively, their dimension is *ca.* 2-3  $\mu\text{m}$ . Interestingly, jar- (Figure 1H, 1K, Figure S8), hollow-sphere (Figure 1I, 1L, Figure S9) and flask-shaped (Figure 1J, Figure S10) structure are obtained at 10°C, 20°C and 30°C respectively. The dimension of the jar- and the hollow-sphere structure is *ca.* 3-5  $\mu\text{m}$ , and the flask-shaped structure is *ca.* 500 nm. These morphology changes are also clearly characterized from the relative fluorescent images. Besides the aggregate structure, the dimension of porphyrin nanostructures would be modulated by assembly temperature as well in Figure S11.

To understand what affecting the distinct assembly structure of CPTNPPs, we observed the droplet templates formed at different temperatures via using the high-speed camera. It is found that the droplet condensates and crystallizes in tree-like

ice crystal (Figure S2) at -20°C, which induces CPTNPP vesicles to assembly by the ice-crystal template, forming a tree-like structure as shown in Figure S3. When improved the assembly temperature to -10°C, the condensed droplets merge/deform (Figure S2), leading to the resultant wavy-like (Figure S4) or honey-comb structure in Figure 1A and Figure S5. When further elevating the assembly temperature over -5°C, the separated droplet template is formed (Figure S2), contributing to the production of the separated assembly structures, such as ring-, skeleton- and cap-shaped structure in Figure 1B (Figure S6), 1C (Figure S7) and 1G. But when the assembly temperature is over 10°C, no condensed droplet is formed on the substrate, which brings about another assembly mechanism: “vesicle template”.

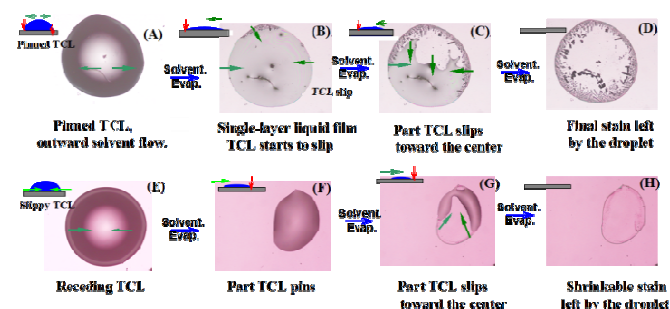


**Figure 2.** *In-situ* optic microscopy images for the stick-slip mode of TCL of droplet evaporation on the (A-D) low- or (E-H) high-temperature substrate. (A, E) The initial droplet with (A) pinned TCL and the outward flow toward the brim aroused from convective evaporation on low-temperature substrate or (E) with receding TCL on high-temperature substrate. (B, F) After droplet with single-layer liquid film formed, the TCL would slip toward the center, (C, G) Part TCL slips toward the center, (D, H) the final stain after the droplet evaporation. The green arrow indicates the flow or slip direction, while the red arrow indicates the pinned TCL. The insert scheme is the side view of the corresponding droplet to better understand the evaporation process.

To clarify the detailed formation mechanism of various CPTNPP nanostructures, we *in-situ* observe the evaporation process for droplet at different temperatures by combining CCD with optic microscopy in **Figure 2** and Figure S12-13. Clearly, the assembly temperature produces an important influence on the resultant deposit morphology.<sup>12</sup> When the droplet is on the low-temperature substrate, its TCL firstly pins accompanied with an obviously outward evaporating flow from the center toward the brim in Figure 2A. The outward flow carries the nonvolatile element to the edge, ensured that liquid evaporating from the edge is replenished by liquid from the interior. After approaching a homogeneous single-layer liquid film in Figure 2B, part TCL of the droplet starts to slip from the brim to the center in Figure 2C, the slipped TCL guides the final evaporation direction of the droplet, leaving an obvious coffee ring structure in Figure 2D. In contrast, when the droplet is on the high-temperature substrate (Figure 2E), the receded TCL causes a great shrinkage for the droplet toward the center. After approaching a single-layer liquid film (Figure 2F), part TCL pins, allowing other part of TCL to slip toward the center accompanied with the solvent evaporation (Figure 2G), leaving a shrinkable stain in Figure 2H. Notably, assembly temperature affects the resultant structure based on changing the stick-slip mode of TCL of droplet, which mainly depends on a competition between pinning force (resistance force from the substrate) and depinning force (capillary force).<sup>12c</sup> The former is determined from the viscosity of the suspension, and the latter is from the evaporation rate. In our case, the improved assembly temperature raises the evaporate rate, but lowers the system's

viscosity, favoring the change of TCL from pinned to slipped state, contributing to a shrinkable and homogeneous film. Vice versa, lowering the assembly temperature contributes to a coffee-ring structure.

Based on the above-mentioned observation of droplet evaporation process in Figure 2, we put forward a possible formation mechanism for various nanostructures from different temperatures in Figure 3. Wherein, temperature's rise enhanced the slide mode of TCL, assembly behavior of CPTNPP, and upward evaporating gas flow, all of these contribute to the formation of different assembly structures. Figure 3(I) illustrates CPTNPP nanostructures assembled from droplet template from  $-5^{\circ}\text{C}$  to  $10^{\circ}\text{C}$ . i.e., CPTNPPs are assembled at the interface between droplet and CPTNPP suspension.<sup>6a-b</sup> In this case, stick-slip mode of droplet (in Figure 3) dominates the resultant nanostructures. When CPTNPP suspension is casted onto the droplet template at  $-5^{\circ}\text{C}$ , the TCL of droplet pins, the convective evaporation process (Figure 2A,3C) carries most of CPTNPP vesicles toward the edge of the droplet (Figure 3C), resulting in the ring-like nanostructures<sup>12,6a</sup> (Figure 3D, 1B). When the sample is casted onto the droplet at  $5^{\circ}\text{C}$  in Figure 3G, the rapid slippery TCL (Figure 2E and 2G) accumulates CPTNPP vesicles toward the center of the droplet, the simultaneous improved upward evaporated gas flow and assembly behavior of CPTNPPs is favorable for the vesicles to coagulate and completely spread around the whole evaporation front of the droplet, forming a vivid copy of the droplet as cap-shaped particles in Figure 3H, 1G. Interestingly, when the sample is assembled at  $0^{\circ}\text{C}$  in Figure 3 E, part slippery TCL leads CPTNPP vesicles to spread toward the center of the droplet, forming multiple ring-shaped structure, while the upward evaporated gas flow makes the formed multi-ring as a skeleton building in Figure 3 F, 1C, which clearly records the slip process of TCL.

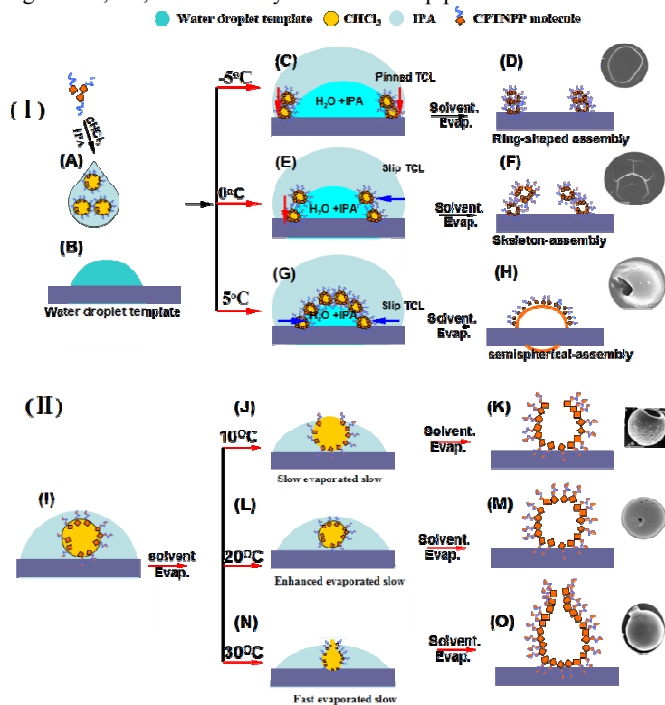


**Figure 3.** Schematic illustration for the morphology evolution process of as-prepared porphyrin nanostructures. Porphyrin assembly based on (I) droplet template from  $-5^{\circ}\text{C}$  to  $10^{\circ}\text{C}$ , and (II) vesicle template at  $10 \sim 30^{\circ}\text{C}$ . For the droplet template approach in (I), increased assembly temperature causes the stick-slip mode of TCL; while for the vesicle template in (II), the rising temperature affects the evaporation solvent flow, all of these contributes to the different aggregate structures.

When the assembly temperature is over  $10^{\circ}\text{C}$ , no droplet condensates on the substrate. In this case, CPTNPPs' assembly mainly depends on the vesicle template<sup>13d</sup> (in Figure 3(II)) owing to the distinct interface tension between chloroform and IPA. This formation process is similar to the solution-solid growth process described by literature.<sup>13d-e</sup> In this case, the rising temperature affects the coagulated behavior of vesicles and solvent evaporated flow, which affects the resultant porphyrin nanostructures. When the sample is assembled at  $10^{\circ}\text{C}$  (Figure 3J), slow evaporation rate only brings solvents upward to causes an opening or many tiny opening in the exterior shell of the vesicle, forming a jar-like structure (in Figure 3K, 1H). While improved assembly temperature ( $20^{\circ}\text{C}$ , Figure 3L) would carry the solvent mixing of CPTNPPs toward the exterior shell, the improved assembly behavior of CPTNPPs allows a timely replenishment toward the opening formed from solvent flow, yielding a perfect hollow particle with gossamer structure around the particle in Figure 3M, 1I. Further raising the assembly temperature ( $30^{\circ}\text{C}$ , Figure 3N) allows solvent evaporation accompanied with more mixing of CPTNPPs, resulted in an continuous assembly of CPTNPPs following the trail line of the evaporated gas flow, formed an additional assembly structure outside the vesicle, i.e., a flask-like structures<sup>13d</sup> in Figure 3O, 1J.

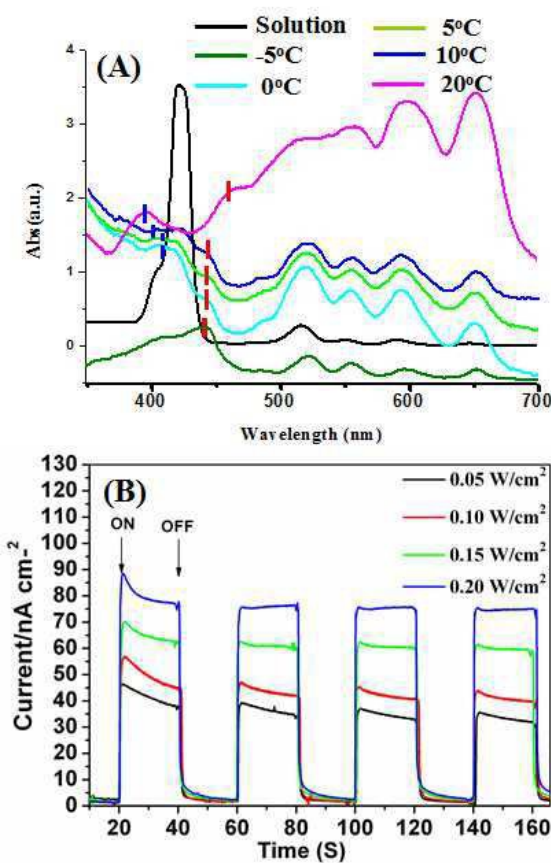


**Figure 4.** (A) UV-Vis absorbance spectra of the samples obtained at different assembly temperature, (B) The photocurrent response of Porphyrin/ITO functionalized electrode, in an argon-saturated  $0.1 \text{ M Na}_2\text{SO}_4$  aqueous solution containing  $50 \text{ mM TEA}$  upon white light irradiation. "On" represents the electrode under light irradiation, while "Off" means the light was turned off.

Various CPTNPPs nanostructures from different temperatures were further evaluated by UV-vis adsorbance spectra of the formed assemblies and the monomeric CPTNPPs in Figure 4A. Compared to the Soret-band of the monomeric CPTNPP dispersed in chloroform (centered at *ca.*  $420 \text{ nm}$ ), the assemblies (from  $-5^{\circ}\text{C}$ )

showed a red-shifted/broadened band at *ca.* 444 nm (Figure 4A), implying that most of CPTNPPs were possibly organized as *J-like* aggregate<sup>5</sup>. In comparison, the assemblies showed a red-shift band at *ca.* 444, 444, 445 and 460 nm (indicated by red bar) when prepared from 0°C, 5°C, 10°C, 20°C respectively, accompanied with a blue-shifted Soret-band at *ca.* 410, 410, 400, 391 nm (indicated by blue bar); implying that most of CPTNPPs were possibly organized as the mixing *J-like* and *H-like* aggregate.<sup>5</sup> Notably, an enhanced blue- or red-shift spectra is observed for the sample assembled at 20°C, and this absorbance band (~ 650 nm) manifests itself with a relatively sharper profile compared to the broad Q band of the monomeric CPTNPP in Figure 4A, indicating the distinct aggregate state. Meantime, the optic-electric properties<sup>13</sup> of the films assembled from spherical porphyrin structure were investigated in Figure 4B. The photoelectrochemical<sup>13</sup> measurements were carried out in an argon-saturated 0.1 M Na<sub>2</sub>SO<sub>4</sub> aqueous solution containing 50 mM triethanolamine (TEA) acting as a sacrificial electron donor<sup>13c</sup> using Porphyrin/ITO as the working electrode, a platinum counter electrode, and an Ag/AgCl (sat. KCl) reference electrode (Hereafter represented by ITO/porphyrin/TEA/Pt systems, respectively, where/ denotes an interface). When Porphyrin/ITO electrode was irradiated with white light with different power density at an applied potential of +0.1V versus Ag/AgCl (saturated KCl), a stable anodic photocurrent from the electrolyte to the ITO electrode appeared. The photocurrent dropped instantly when the illumination was cut off.

## Conclusions

In conclusion, a variety of porphyrin assembly structures were facilely obtained based on the droplet template by just varying the assembly temperature. The assembly structures cover tree-like, honey-comb, ring-, skeleton-, jar-, hollow spheric and flask-like. The distinct assembly mechanism is clarified. The as-fabricated structure showed special optic-electric properties. This is of great significance for the design and fabrication of various porphyrin assembly structures.

The authors would like to thank the NSFC (Grant Nos. 50973117, 21074139, 91127029 and 51373183), the 973 Program (2013CB933004, 2011CB932303 and 2011CB808400) for continuous financial support. And Prof. J. Cai would like to thank the financial support from the Natural Science Foundation (20142BAB203003) and technological support projects of Jiangxi Province (20142BBG70004).

## Notes and references

<sup>a</sup> Laboratory of Bio-inspired Smart Interface Sciences, Technical Institute of Physics and Chemistry, Chinese Academy of Sciences (CAS), Beijing 100190, P. R. China;

E-mail: jingxiawang@mail.ipc.ac.cn, wangzhang@iccas.ac.cn

<sup>b</sup> Key Laboratory of Green Printing, The Laboratory of Organic Solids, Institute of Chemistry, CAS, Beijing, China, 100190.

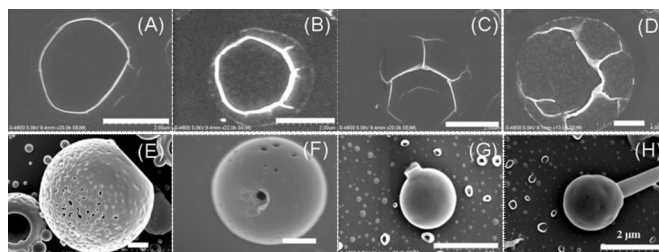
<sup>c</sup> College of Chemistry & Chemical Engineering, Jinggangshan University, Jian, Jiangxi Province P. R. China, 343009.

†Electronic Supplementary Information (ESI) available: [details of synthesis of CPTNPPs, assembly morphology, droplet template, evaporation process for droplet template]. See DOI: 10.1039/c000000x/

- 1 a) C. M. Drain, A. Varotto, I. Radivojevic, *Chem. Rev.* 2009, **109**, 1630; b) H. B. Liu, J. L. Xu, Y. J. Li, Y. L. Li, *Acc. Chem. Res.* 2010, **43**, 1496; c) Z. C. Wan, K. C. J. Ho, C. J. Medforth, J. A. Shelhutt, *Adv. Mater.* 2006, **18**, 2557; d) K. K. Ng, J. F. Lovell, A. Vedadi, T. Hajian, G. Zheng, *Acs Nano.* 2014, **7**, 3484; e) Y. Liu, Q. Q. Shi, L. C. Ma, H. L. Dong, J. H. Tan, W. P. Hu, X. W. Zhan, *J. Mater. Chem. C* 2014, **2**, 9505.
- 2 a) Y. Qiu, P. Chen, M. Liu, *J. Am. Chem. Soc.* 2010, **132**, 9644; b) P. Guo, P. Chen, M. Liu, *ACS Appl. Mater. & Interf.* 2013, **5**, 5336; c) P. Guo, P. Chen, W. Ma, M. Liu, *J. Mater. Chem.* 2012, **22**, 20243; P. Guo, P. Chen, M. Liu, *Langmuir* 2012, **28**, 15482.
- 3 a) T. Hirose, F. Helmich, E. W. Meijer, *Angew. Chem. Int. Ed.* 2013, **52**, 304; b) J. Hu, Y. Guo, H. Liang, L. Wan, L. Jiang, *J. Am. Chem. Soc.* 2005, **127**, 17090; c) Y. Gao, X. Zhang, C. Ma, X. Li, J. Jiang, *J. Am. Chem. Soc.*, 2008, **130**, 17044; d) G. Lu, Y. Chen, Y. Zhang, M. Bao, Y. Bian, X. Li, J. Jiang, *J. Am. Chem. Soc.* 2008, **130**, 11623.
- 4 a) W. Lv, X. Zhang, J. Lu, Y. Zhang, X. Li, J. Jiang, S. Eur. *J. Inorg. Chem.* 2008, 2455; b) T. Hasoe, H. Oik, A. S. D. Sandanayaka, H. Murata, *Chem. Commun.* 2008, 724; c) Z. Wang, C. J. Medforth, *J. Am. Chem. Soc.* 2004, **126**, 15954; d) L. Wang, Y. L. Chen, J. Z. Zhang, *Nanoscale*, 2014, **6**, 1871.
- 5 a) P. Guo, G. Zhao, P. L. Chen, B. Lei, L. Jiang, H. Zhang, W. Hu, M. Liu, *Acs Nano* 2014, **8**, 3402; b) Y. Zhang, P. Chen, M. Liu, *Chem. Eur. J.* 2008, **14**, 1793; c) R. Teixeira, S. M. Andrade, V. V. Serra, P. M. R. Paulo, R. Sanchez-Coronilla, M. G. P. M. S. Neves, J. A. S. Cavaleiro, S. M. B. Costa, *J. Phys. Chem. B* 2012, **116**, 2396; d) L. Wang, X. Xie, W. Zhang, J. Zhang, M. Zhu, Y. Guo, P. Chen, M. Liu, G. Yu, *J. Mater. Chem. C* 2014, **2**, 6484.
- 6 a) J. Cai, S. Chen, L. Cui, C. Chen, P. Chen, J. Wang, D. Wang, Y. Song, L. Jiang, *Adv. Mater. Interf.* 2014, Doi:10.1002/admi.201400365; b) T. Wang, J. Cai, F. Jin, L. Cui, Y. Zheng, J. Wang, Y. Song, L. Jiang, *Chem. Commun.* 2015, **51**, 1367.
- 7 a) L. S. Wan, L. W. Zhu, O. Yang and Z. K. Xu, *Chem. Commun.* 2014, **50**, 4024; b) H. Bai, C. Du, A. J. Zhang, and L. Li, *Angew. Chem. Int. Ed.* 2013, **52**, 2; c) L. Qu, G. Shi, F. Chen, J. Zhang, *Macromolecules* 2003, **36**, 1063.
- 8 a) J. Y. Yuan, L. T. Qu, D. Q. Zhang, G. Q. Shi, *Chem. Commun.* 2004, 994; b) W. Li, Y. Nie, J. Zhang, D. Zhu, X. Li, H. Z. Sun, K. Yu, B. Yang, *Macromol. Chem. Phys.* 2008, **209**, 247.
- 9 a) T. S. Wong, S. H. Kang, S. K. Y. Tang, E. J. Smythe, B. D. Hatton, E. J. Smythe, A. Grinthal, J. Aizenberg, *Nature* 2011, **477**, 443; b) W. Han, Z. Lin, *Angew. Chem. Int. Ed.* 2012, **51**, 1534; c) S. W. Hong, M. Byun, Z. Q. Lin, *Angew. Chem. Int. Ed.* 2009, **48**, 512; c) M. Byun, W. Han, B. Li, X. Xin, Z. Lin, *Angew. Chem. Int. Ed.* 2013, **52**, 1122.
- 10 a) B. Su, C. Zhang, S. Chen, X. Zhang, L. Chen, Y. Wu, Y. Nie, Y. Song, L. Jiang, *Adv. Mater.* 2014, **26**, 2501; b) Y. Wu, B. Su, L. Jiang, J. Heeger, *Adv. Mater.* 2013, **25**, 6526; c) J. X. Wang, L. B. Wang, Y. L. Song, L. Jiang, *J. Mater. Chem. C* 2013, **1**, 6048.
- 11 a) T. Sun, G. Qing, B. Su, L. Jiang, *Chem. Soc. Rev.* 2011, **40**, 2909; b) M. Kuang, J. Wang, B. Bao, F. Li, L. Wang, L. Jiang, Y. Song, *Adv. Opt. Mater.* 2014, **2**, 34; c) Y. Huang, J. Zhou, B. Su, L. Shi, J. Wang, S. Chen, L. Wang, J. Zi, Y. Song, L. Jiang, *J. Am. Chem. Soc.* 2012, **134**, 17053.

- 12 a) R. D. Deegan, O. Bakajin, T. F. Dupont, G. Huber, S. R. Nagel, T. A. Witten, *Nature* 1997, **389**, 827; b) P. J. Yunker, T. Still, M. A. Lohr, A. G. Yodh, *Nature* 2011, **476**, 308; c) J. Xu, J. Xia, S. Hong, Z. Q. Lin, F. Qiu, and Y. Yang, *Phys. Rev. Lett.* 2006, **96**, 066104.
- 13 a) F. Zhang, K. Jiang, J. Huang, C. Yu, S. Li, M. Chen, L. Yang, Y. Song, *J. Mater. Chem. A* 2013, **1**, 4858; b) V. Chukharev, T. Vuorinen, A. Efimov, and N. V. Tkachenko, M. Kimura and S. Fukuzumi, H. Imahori, H. Lemmetyinen. *Langmuir* 2005, **21**, 6385; c) H. Yamada, H. Imahori, Y. Nishimura, I. Yamazaki, T. K. Ahn, S. K. Kim, D. Kim, and S. Fukuzumi. *J. Am. Chem. Soc.* 2003, **125**, 9129; d) C. Huang, L. Wen, H. Liu, Y. Li, X. Liu, M. Yuan, J. Zhai, L. Jiang, D. Zhu, *Adv. Mater.* 2009, **21**, 1721; e) A.-W. Xu, Y.-P. Fang, L.-P. You, H.-Q. Liu, *J. Am. Chem. Soc.* 2003, **125**, 1494.

## Topic of content



Facile fabrication of various porphyrin nanostructures from oil-aqueous interface by changing the assembly temperature, the structure covers of tree-, wavy-, honey-comb, ring-, skeleton-, jar-, hollow spherical and flask-like.